A framework for understanding drag parameterizations for coral reefs

Johanna H. Rosman[1] and James L. Hench[2]

[1]   In a hydrodynamic sense, a coral reef is a complex array of obstacles that exerts a net drag force on water moving over the reef. This drag is typically parameterized in ocean circulation models using drag coefficients (C_D) or roughness length scales (z_0); however, published C_D for coral reefs span two orders of magnitude, posing a challenge to predictive modeling. Here we examine the reasons for the large range in reported C_D and assess the limitations of using C_D and z_0 to parameterize drag on reefs. Using a formal framework based on the 3-D spatially averaged momentum equations, we show that C_D and z_0 are functions of canopy geometry and velocity profile shape. Using an idealized two-layer model, we illustrate that C_D can vary by more than an order of magnitude for the same geometry and flow depending on the reference velocity selected and that differences in definition account for much of the range in reported C_D values. Roughness length scales z_0 are typically used in 3-D circulation models to adjust C_D for reference height, but this relies on spatially averaged near-bottom velocity profiles being logarithmic. Measurements from a shallow backreef indicate that z_0 determined from fits to point measurements of velocity profiles can be very different from z_0 required to parameterize spatially averaged drag. More sophisticated parameterizations for drag and shear stresses are required to simulate 3-D velocity fields over shallow reefs; in the meantime, we urge caution when using published C_D and z_0 values for coral reefs.

Citation: Rosman, J. H., and J. L. Hench (2011), A framework for understanding drag parameterizations for coral reefs, *J. Geophys. Res.*, *116*, C08025, doi:10.1029/2010JC006892.

1.   Introduction

[2]   Corals depend on water motion for delivery of particles, nutrients, and dissolved gases; for removal of waste products; and for larval transport. Respiration, photosynthesis, and calcification rates of corals increase with flow speed thereby affecting colony growth rates and morphologies [*Todd*, 2008]. Wave and current conditions affect prey capture by corals [*Sebens et al.*, 1998] and nutrient uptake rates by reef assemblages [*Thomas and Atkinson*, 1997]. Reef-scale circulation patterns determine dispersal and retention of water within reef systems, thereby affecting connectivity among populations [*Cowen and Sponaugle*, 2009]. Hence, there is considerable interest in describing and modeling flow over coral reefs at scales ranging from flow within an individual coral colony [e.g., *Kaandorp et al.*, 2003; *Chang*, 2007] to circulation within reef-lagoon systems [e.g., *Prager*, 1991; *Hench et al.*, 2008; *Lowe et al.*, 2009].

[3]   Corals have irregular, branching morphologies and reef topography varies at scales ranging from centimeters to kilometers (Figure 1), therefore flow within these systems is complex. There has been some effort to quantify the small-scale spatial structure of reefs [*Roberts et al.*, 1975; *Nunes and Pawlak*, 2008; *Zawada et al.*, 2010]; however, the connection between the physical roughness of reefs and the hydrodynamic roughness (or bottom drag) acting on currents and waves is not well understood.

[4]   In circulation models, variability in reef geometry occurs at scales smaller than the resolution of the computational grid; thus, drag due to the small-scale geometry must be parameterized. In most existing circulation models, this is done using a quadratic drag law in which the depth-averaged drag force (F_D) or the effective bottom shear stress ($\tau_{b,\mathrm{eff}}$) is related to the depth-averaged velocity or the velocity at a reference height above bottom. We use $\tau_{b,\mathrm{eff}}$ because, for the case of a very rough boundary, the bottom boundary condition on shear stress is not the true stress but rather represents net drag. The standard quadratic drag law is

$$F_D = \frac{\tau_{b,\mathrm{eff}}}{H} = \frac{\rho\, u_{*,\mathrm{eff}}^2}{H} = \frac{\rho C_D U_{\mathrm{ref}}^2}{H}, \tag{1}$$

where ρ is the density of water, $u_{*,\mathrm{eff}}$ is the effective shear velocity (corresponding to $\tau_{b,\mathrm{eff}}$), C_D is the bulk drag coefficient, U_{ref} is a reference velocity (depth-integrated velocity or velocity at some height above bottom), and H is the water column height. Traditionally, drag coefficients estimated from field measurements have used the velocity at 1 m above

[1]Institute of Marine Sciences, University of North Carolina at Chapel Hill, Morehead City, North Carolina, USA.
[2]Duke University Marine Laboratory, Nicholas School of the Environment, Beaufort, North Carolina, USA.
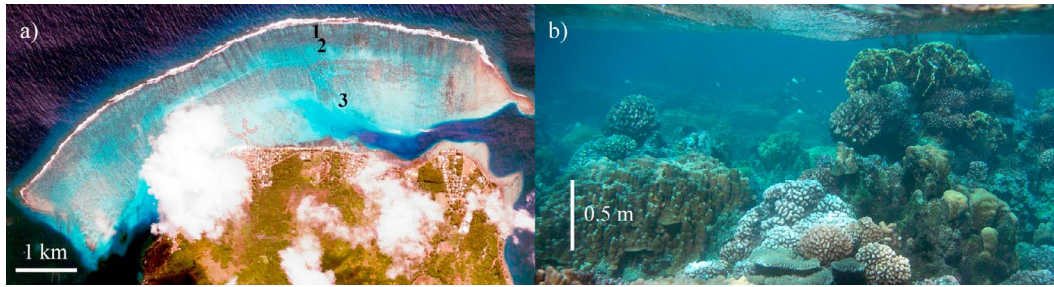
Figure 1. (a) Aerial photograph of the backreef on the north shore of Moorea with numbers marking cross-reef measurement array. (b) Underwater photograph of the reef near Station 2.

bottom for U_{ref} [e.g., *Sternberg*, 1968; *Gross and Nowell*, 1983]. For corals reefs, defining drag coefficients is complicated because solid obstructions occupy a layer above the true bottom and there is flow through the coral layer as well as above it.

[5] Experimental studies on coral reefs have estimated drag coefficients from log fits to velocity profiles [*Reidenbach et al.*, 2006; *Jones et al.*, 2008], from measurements of Reynolds stress [*Lowe et al.*, 2005; *Reidenbach et al.*, 2006; *Tarya et al.*, 2010], or by assuming a drag and pressure gradient momentum balance and calculating C_D from surface level or pressure measurements [*Bilger and Atkinson*, 1992; *Baird and Atkinson*, 1997; *Thomas and Atkinson*, 1997; *McDonald et al.*, 2006; *Coronado et al.*, 2007; *Hench et al.*, 2008]. Drag coefficients for simulations of flow over coral reefs have been based on values reported from field and laboratory measurements [*Hearn*, 1999] or selected to tune models to match measured surface elevations or currents [*Young et al.*, 1994; *Kraines et al.*, 1998; *Tamura et al.*, 2007; *Lowe et al.*, 2009].

[6] Pressure gradients due to surface waves drive periodic flow through a coral layer [*Lowe et al.*, 2005], resulting in increased turbulence and enhanced momentum exchange between the canopy layer and overlying water column [*Reidenbach et al.*, 2007]. In turn, this leads to larger currents through the coral canopy, and hence larger drag, which is often parameterized by using a C_D or z_0 that is dependent on wave conditions [*Grant and Madsen*, 1979]. Even in the absence of waves, reported drag coefficients for coral reefs vary from 0.01 [*Reidenbach et al.*, 2006] to 0.8 [*McDonald et al.*, 2006] (Table 1). As friction is often a dominant term in the momentum balance over shallow reefs, circulation patterns calculated using numerical models can be very sensitive to the drag parameterization used [*Kunkel et al.*, 2006; *Tarya et al.*, 2010]. Drag coefficients used in reef circulation models range from 0.02 to 0.1 (Table 2). The broad range of reported drag coefficient values thus presents a significant challenge to predictive modeling.

[7] *McDonald et al.* [2006] proposed that the wide range of drag coefficients in the literature could be explained by a dependence of C_D on the ratio of coral canopy height (h) to water depth (H) and presented an empirical expression for this dependence. Their empirical result was largely based on laboratory flume experiments with a 20 cm canopy of *Porites*

Table 1. Comparison of Published C_D and z_0 From Measurements on Coral Reefs, Along With Reference Velocities Used for the Parameterization, and Flow and Canopy Parameters Relevant to the Two-Layer Model[a]

	Drag Parameter	U_{ref}	U_2/U_1	h/H	λ_F	γ
	C_D					
Porites compressa[b] [*Baird and Atkinson*, 1997]	0.04–0.06	$\overline{u}\vert_{z=H}$	–	0.4	–	–
Porites compressa[b] [*Thomas and Atkinson*, 1997]	0.06–0.1	$\overline{u}\vert_{z=H}$	–	0.22	–	–
Acropora palmate [*Lugo-Fernandez et al.*, 1998]	0.06–0.2	$\overline{u}\vert_{z=0.6m}$	–	–	–	–
Sand with coral outcrops [*Baird et al.*, 2004]	0.036	U	–	0.2–0.5	–	–
Porites compressa[b] [*McDonald et al.*, 2006]	0.06–0.8	Q/A_{flume}	–	0.45–0.9	–	–
Porites compressa[c] [*McDonald et al.*, 2006]	0.016–0.05	$\overline{u}\vert_{z=H}$	–	0.45–0.9	–	–
Corals, seagrass, sand [*Coronado et al.*, 2007]	0.015	U	–	~0.05	–	–
	C_f					
PVC cylinders[b] [*Lowe et al.*, 2005]	0.009	$\overline{u}\vert_{z=0.25m}$	0.1	0.25	0.50	0.8
	0.015	$\overline{u}\vert_{z=0.25m}$	0.22	0.25	0.22	0.91
	0.015	$\overline{u}\vert_{z=0.25m}$	0.32	0.25	0.12	0.95
Varied: corals, soft corals, anemones, sponges [*Reidenbach et al.*, 2006]	0.01–0.015	$\overline{u}\vert_{z=1m}$	–	~0.01	–	
Pocillopora sp., *Porites sp.* [*Jones et al.*, 2008]	0.015	U	–	–	–	
Unknown reef type [*Tarya et al.*, 2010]	0.017–0.027	U	–	–	–	
	z_0					
Varied, see entry above [*Reidenbach et al.*, 2006]	0.01–0.04 m	n/a	–	~0.01	–	

[a]Blank entries indicate that information was not available. Symbols are defined in the notation section.
[b]Reported C_D have been divided by two here because an additional factor of 2 was used in the original definitions.
[c]Alternative C_D computed here from pressure gradients and near-surface velocities of *McDonald et al.* [2006].

Table 2. Comparison of Drag Parameterizations Used for Numerical Models of Flow Over Coral Reefs in the Literature[a]

	Drag Parameter	U_{ref}
	C_D	
Hearn [1999]	$C_D = 0.1$	U
Kunkel et al. [2006]	$C_D = 0.05$	U
Tamura et al. [2007]	$C_D = 0.035$	U
Tarya et al. [2010]	$C_D = 0.021$	U
	z_0	
Young et al. [1994]	$z_0 = 0.01, 0.08$ m	N/A
Tartinville et al. [1997]	$z_0 = 0.04, 0.08$ m	N/A
Lowe et al. [2009]	$z_0 = 0.017$ m	N/A
	Other	
Manning's n [*Prager*, 1991]	$n = 0.05$	U
Linear drag coefficient R [*Symonds et al.*, 1995]	$R = 0.08$ m s^{-1}	U
Manning's n [*Kraines et al.*, 1998, 1999]	$n = 0.1$ ($C_D = 0.0026$–0.042)	U

[a]Symbols are defined in the notation section.

compressa and C_D was defined using the bulk flow rate divided by flume cross-sectional area. However, some field measurements for which C_D was defined differently [*Reidenbach et al.*, 2007] were also included in the fit. The empirical relationship proposed by *McDonald et al.* [2006] is unique to both the definition of C_D and the particular coral canopy used.

[8] A number of different drag parameterizations have been used in the literature. For example, some studies have parameterized the shear stress at the top of the canopy [*Lowe et al.*, 2005; *Reidenbach et al.*, 2006], while others have parameterized the net drag within the canopy [*McDonald et al.*, 2006; *Hench et al.*, 2008]. Some studies have used the depth-integrated velocity [*Hench et al.*, 2008] and others have used the near-surface velocity [*Bilger and Atkinson*, 1992; *Baird and Atkinson*, 1997; *Thomas and Atkinson*, 1997] or the velocity at a fixed height above bottom [*Lowe et al.*, 2005; *Reidenbach et al.*, 2006] for the reference velocity. In some cases, differently defined C_D values have been compared [e.g., *McDonald et al.*, 2006; *Monismith*, 2007; *Tarya et al.*, 2010], and measured C_D values have been used in numerical models without taking into account differences in the C_D definition [e.g., *Hearn*, 1999; *Kunkel et al.*, 2006].

[9] The main objectives of this paper are (1) to relate C_D and z_0 quantitatively to the physics they represent, (2) to use this framework to assess whether differences in definition contribute to the wide range of C_D in the literature, and (3) to assess the limitations of using C_D or z_0 to parameterize drag on coral reefs. For simplicity, the discussion is limited to reefs without waves, such as shallow reef flats and backreefs beyond the zone of wave breaking. Using a simple two-layer conceptual model we illustrate the dependence of C_D on the definition used, and the dependence of C_D on canopy geometry and the shape of velocity profiles. We show that discrepancies among reported drag coefficients are due, in part, to differences in the way C_D is defined. We evaluate the use of bulk C_D and z_0 to parameterize drag with data from a shallow backreef in Moorea, French Polynesia, where the momentum balance is dominated by pressure gradient and

drag terms. Finally, we discuss the implications of specifying a z_0 to define the bottom drag condition in 3-D models of flow over and through a reef.

2. Conservation Equations and Conceptual Model

2.1. Complete Three-Dimensional Momentum Equations

[10] For flow in regions with significant spatial variations, such as within coral canopies, it is useful to average the Navier-Stokes equations over a volume that is large compared with random spatial variations but small compared with gradients in the larger-scale flow. For the case of flow over a rough boundary, the most appropriate averaging volume is the fluid within a cuboid that is very thin in the vertical compared with the horizontal; thus, averages are performed horizontally over many roughness elements (e.g., many coral branches and colonies) but gradients in the vertical are resolved. The distribution of obstacles (e.g., height, spacing) and flow properties (e.g., velocity, pressure) can vary randomly within the averaging volume but should not vary significantly in a systematic way across the averaging volume. From a practical standpoint, this means that averaging volumes on reefs should usually be large (wide) compared with individual coral colonies, but small compared with larger (reef) scale variations in coral density, water depth, and flow speed. Typical averaging volumes on reefs are therefore likely to be 10 s to 100 s of meters in width.

[11] Assuming mean shear stress gradients in the vertical are much larger than those in the horizontal, the spatially averaged momentum equation in the x direction is [e.g., *Nikora et al.*, 2007],

$$\underbrace{\frac{\partial \langle \overline{u} \rangle}{\partial t} + \langle \overline{u} \rangle \frac{\partial \langle \overline{u} \rangle}{\partial x} + \langle \overline{v} \rangle \frac{\partial \langle \overline{u} \rangle}{\partial y} + \langle \overline{w} \rangle \frac{\partial \langle \overline{u} \rangle}{\partial z}}_{\text{acceleration}}$$

$$= \underbrace{-\frac{1}{\rho \gamma} \frac{\partial (\gamma \langle \overline{p} \rangle)}{\partial x}}_{\substack{\text{pressure gradient} \\ \text{force}}} + \underbrace{\frac{1}{\rho \gamma} \frac{\partial (\gamma \tau_{xz})}{\partial z}}_{\substack{\text{shear stress} \\ \text{gradient force}}} - \underbrace{f_{Fx}}_{\text{form drag}} - \underbrace{f_{Vx}}_{\text{viscous drag}}, \quad (2)$$

where

$$\tau_{xz} = \underbrace{-\rho \langle \overline{u'w'} \rangle}_{\text{Reynolds stress}} \underbrace{-\rho \langle \overline{u}''\overline{w}'' \rangle}_{\text{dispersive stress}} + \underbrace{\mu \frac{\partial \langle \overline{u} \rangle}{\partial z}}_{\text{viscous stress}}$$

$$f_{Fx} = -\frac{1}{\rho \Gamma_{fl}} \int_S \overline{p} n_x \, dS$$

$$f_{Vx} = \frac{v}{\Gamma_{fl}} \int_S \frac{\partial \overline{u}}{\partial x} n_x + \frac{\partial \overline{u}}{\partial y} n_y + \frac{\partial \overline{u}}{\partial z} n_z \, dS.$$

[12] Each term in equation (2) has units of force per unit fluid mass. x, y, z are orthogonal coordinates with z positive upwards, u, v, w are the velocity components in directions x, y, z, respectively, and the unit normal to the solid surface has components n_x, n_y, n_z. The fluid density is ρ, the molecular viscosity is μ and ν is the kinematic viscosity. The porosity, γ, is defined as the volume of fluid (Γ_{fl}) within the averaging cuboid divided by the total cuboid volume (Γ) and can vary with x, y, z. Over-bars indicate time averages in the Reynolds-
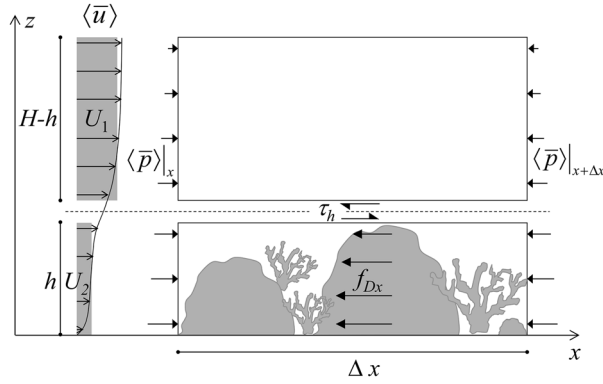
Figure 2. Schematic diagram of idealized two-layer model of flow over and through a coral reef. The upper layer (height H-h) is entirely fluid while the lower layer (height h) contains solid obstacles.

averaged sense. Angular brackets indicate spatial averages over the averaging volume, e.g., $\langle \theta \rangle = \Gamma_{fl}^{-1} \iiint_{\Gamma_{fl}} \theta \, dV$. Single primes indicate deviations from the time average ($u' = \overline{u} - u$) and double primes indicate deviation from the spatial average ($\overline{u}'' = \langle \overline{u} \rangle - \overline{u}$).

[13] The shear stress, τ_{xz} (denoting stress in the x direction exerted by fluid above and below a given averaging volume) is the sum of the viscous stress, the Reynolds stress and the dispersive stress. The dispersive stress is the spatial analog of the Reynolds stress. While the Reynolds stress represents the transport of momentum due to the time-averaged effect of turbulent fluctuations, the dispersive stress represents the transport of momentum due to the spatially averaged effects of persistent spatial variations in the flow. The form drag, f_{Fx}, and viscous drag, f_{Vx}, result from integrating the pressure gradient and viscous stress terms, respectively, around solid obstacle surfaces in the interior of the averaging volume; each represents a drag force per unit fluid mass. On coral reefs, form drag is typically much larger than viscous drag. Henceforth, we use f_{Dx} to represent $f_{Fx} + f_{Vx}$.

[14] In order to compute three-dimensional information about velocity fields using equation (2), parameterizations for the drag and stress gradient terms are required. While some progress has been made on parameterizing these terms for terrestrial forest and urban canopies [e.g., *Raupach and Thom*, 1981; *Coceal and Belcher*, 2004] and seagrass canopies [*Ghisalberti and Nepf*, 2004], little progress has been made on stress and drag parameterizations for coral reefs in which a wide range of roughness length scales exists, roughness length scales can be similar to boundary layer turbulence length scales, and solid obstructions can occupy a significant fraction of the water column. In this paper, we consider simplified drag parameterizations commonly used in ocean circulation models, which result from vertically integrating the drag term in equation (2) over the layer containing solid obstacles.

2.2. Depth-Averaged Momentum Equations

[15] A simplified momentum balance can be obtained by vertically integrating equation (2). For simplicity, we consider unidirectional flow (direction invariant with z) in the

positive x direction with no gradients in the cross-flow (y) direction (Figure 2). We assume that $\langle \overline{p} \rangle$ is hydrostatic and that there is no surface wind stress. There are two possible approaches to deriving equations for the depth-integrated flow: integrating over the complete water column, and integrating only over the layer above the coral canopy.

2.2.1. Depth-Integrated Model for Whole Water Column

[16] If equation (2) is integrated over the entire water column volume, including the canopy layer (Figure 2), all friction (skin friction and form drag) is included in the drag term. The result is,

$$\frac{\partial U}{\partial t} + U\frac{\partial U}{\partial x} + \frac{1}{H_{\text{eff}}}\int_0^H \left(\tilde{u}\frac{\partial \tilde{u}}{\partial x} + \tilde{w}\frac{\partial \tilde{u}}{\partial z} \right)\gamma \, dz$$
$$= -g\frac{\partial \eta}{\partial x} - \underbrace{\frac{1}{H_{\text{eff}}}\int_0^h f_{Dx}\gamma \, dz}_{\text{drag due to canopy layer}} . \tag{3}$$

where $H_{\text{eff}} = \int_0^H \gamma \, dz$ is the effective water column height, equal to the total volume of fluid per unit plan (bottom) area and η is the free surface elevation. The depth-averaged velocity is defined $U = (1/H_{\text{eff}}) \int_0^H \langle \overline{u} \rangle \, \gamma \, dz$. $\tilde{u} = \langle \overline{u} \rangle - U$, and $\tilde{w} = \langle \overline{w} \rangle$ are deviations of the velocity components at height z from the depth average. The effect of the rough boundary is included in the final depth-averaged drag term. In depth-averaged ocean circulation models, the net drag force in equation (3) is often thought of as an effective bottom stress ($\tau_{b,\text{eff}}$); i.e.,

$$\frac{1}{H_{\text{eff}}}\int_0^h f_{Dx}\gamma \, dz \equiv \frac{\tau_{b,\text{eff}}}{\rho H_{\text{eff}}} \equiv \frac{u_{*,\text{eff}}^2}{H_{\text{eff}}}. \tag{4}$$

[17] The depth-integrated volume occupied by solid obstacles is typically small compared with the depth-integrated volume occupied by water; thus, $H_{\text{eff}} \approx H$.

2.2.2. Depth-Integrated Model for Water Column Above Canopy

[18] If, instead of integrating over the entire water column, equation (2) is integrated only over the water column above the coral canopy (Figure 2), the result is

$$\frac{\partial U_1}{\partial t} + U_1\frac{\partial U_1}{\partial x} + \frac{1}{H-h}\int_h^H \left(\tilde{u}\frac{\partial \tilde{u}}{\partial x} + \tilde{w}\frac{\partial \tilde{u}}{\partial z} \right)dz = -g\frac{\partial \eta}{\partial x} - \frac{\tau_h}{\rho(H-h)}. \tag{5}$$

where the depth-integrated velocity above the canopy is defined $U_1 = \frac{1}{(H-h)} \int_h^H \langle \overline{u} \rangle \, dz$, and τ_h is the shear stress at the top of the canopy. Using this approach, the effect of the rough boundary layer on the overlying water column is through the shear stress at the top of the canopy, τ_h, which includes viscous, turbulent and dispersive stress terms but is usually dominated by turbulent stresses [e.g., *Cheng and Castro*, 2002] (Figure 2). If the canopy occupies a small fraction of the water column ($h/H \ll 1$), then $U_1 \approx U$ and $H - h \approx H_{\text{eff}}$; the two forms of the depth-integrated equations (equations (3) and (5)) converge and $\tau_{b,\text{eff}} = \tau_h$.

2.3. Standard Form of the 3-D Momentum Equations

[19] In three-dimensional ocean circulation models, which typically do not explicitly account for small-scale spatial variability or solid obstacles, the form drag and viscous drag terms in equation (2) are omitted and the frictional resistance of the bottom is included instead through the boundary condition on the shear stress at $z = 0$. That is, the x direction momentum equation (again assuming flow only in the x direction) is

$$\frac{\partial \overline{u}}{\partial t} + \overline{u}\frac{\partial \overline{u}}{\partial x} = -\frac{1}{\rho}\frac{\partial \overline{p}}{\partial x} + \frac{1}{\rho}\frac{\partial \tau_{xz}}{\partial z}, \qquad (6)$$

and the bottom shear stress boundary condition is

$$\left.\frac{\tau_{xz}}{\rho}\right|_{z=0} = \frac{\tau_{b,\text{eff}}}{\rho} = \int_0^h f_{Dx}\, \gamma\, dz. \qquad (7)$$

3. Formulation of the Bulk Drag Coefficient

[20] The drag term that arises from each of the above approaches is typically parameterized using a quadratic drag law that relates the bottom drag to the depth-averaged velocity or the velocity at some height in the water column. In this section, we consider the ways in which the drag term in the 2-D and 3-D momentum equations is typically parameterized in order to express C_D and z_0 in terms of the physics they represent. This development is used to consider relationships among different drag parameterizations, in particular, different C_D definitions in the literature.

3.1. Bulk Drag Coefficient Definition in the Two-Dimensional Momentum Equations

3.1.1. Depth-Averaged Model for Whole Water Column

[21] In 2-D (depth-averaged) models, bottom drag is usually parameterized using a bulk drag coefficient $C_D|^U$ that relates the drag term in equation (3) to the depth-averaged velocity U. Again, if flow is unidirectional (in the x direction) over the entire water column, then $C_D|^U$ is defined:

$$F_D = \frac{1}{H_{\text{eff}}}\int_0^h f_{Dx}\, \gamma\, dz \equiv \frac{C_D|^U U^2}{H_{\text{eff}}}. \qquad (8)$$

[22] Here U is the reference velocity for the drag parameterization. If the complete 3-D velocity and pressure distributions and roughness geometry were known, $C_D|^U$ could be computed directly from the drag terms in equation (2); however, in practice, this information is not available. For a canopy with frontal area per unit fluid volume a, f_{Dx} is usually modeled using [e.g., Nepf, 1999],

$$f_{Dx} = \frac{1}{2}c_d\, a\, \langle \overline{u} \rangle^2. \qquad (9)$$

[23] Note that the sectional drag coefficient, c_d, which relates the form drag on an individual obstacle or obstacle array at height z to the fluid velocity and obstacle frontal area at that height, is different from C_D, which is used to parameterize the total depth-integrated drag on a fluid per unit plan (bottom) area. The value of c_d depends on the geometry of the obstacle(s) as well as properties of the incident flow. The sectional drag coefficient c_d is approximately unity for an isolated, infinitely tall, smooth cylinder (diameter d) in a steady flow with $\text{Re} = \langle \overline{u} \rangle d/v = 10^3 - 10^5$ [e.g., Kundu, 1990]. However, c_d varies with Re and can also differ from unity for finite length obstacles [Ghisalberti and Nepf, 2004], near solid boundaries [Nepf and Vivoni, 2000], and within canopy layers where the flow incident on individual obstacles is affected by obstacles upstream [Nepf, 1999]. In general, it is reasonable to assume c_d is of order one. If equation (9) is used to parameterize the drag within the canopy, then $C_D|^U$ is given by

$$C_D|^U = \frac{1}{U^2}\int_0^h \frac{1}{2}\, c_d a\langle \overline{u} \rangle^2\gamma\, dz. \qquad (10)$$

[24] For the same rough boundary, U is likely to increase relative to the within-canopy flow speed as water depth increases; thus, for a given rough boundary $C_D|^U$ is expected to decrease with water depth. Previously, Manning's equation has been used to compute $C_D|^U$ as a function of water depth [Prager, 1991; Kraines et al., 1998, 1999]. However, this empirical equation (which gives a $C_D \sim H^{-1/3}$ dependence) was developed for open channel flow over sand grain roughness and is unlikely to provide accurate drag coefficient estimates for reefs.

3.1.2. Depth-Averaged Model for the Water Column Above the Canopy

[25] If the depth-average is computed only over the layer above solid obstacles, the bottom friction due to the canopy appears in the momentum equation as the shear stress at the top of the canopy (equation (5)). In this approach, the shear stress term is parameterized with a friction coefficient, $C_f|^{U1}$, as

$$\frac{\tau_h}{\rho} \equiv C_f|^{U_1} U_1^2, \qquad (11)$$

where U_1, the depth-averaged velocity above the canopy, is the reference velocity for the drag parameterization. If the canopy occupies a small fraction of the water column ($h/H \ll 1$, $U_1 = U$, $\tau_h = \tau_{b,\text{eff}}$), then $C_f|^{U1} = C_D|^U$ and the two drag parameterizations are equivalent.

3.2. Bulk Drag Coefficient Definition in the Three-Dimensional Momentum Equations

[26] In a 3-D representation of flow over a rough boundary, the bottom boundary condition for τ_{xz} (representing the net bottom drag, equations (6) and (7)) can be parameterized using a reference velocity at any height above bottom; i.e.,

$$\left.\frac{\tau_{xz}}{\rho}\right|_{z=0} = \frac{\tau_{b,\text{eff}}}{\rho} = \int_0^h f_{Dx}\gamma\, dz = C_D|^{U_{\text{ref}}} U_{\text{ref}}^2. \qquad (12)$$

[27] There is a continuous range of choices for U_{ref}. For example, Reidenbach et al. [2006] used the velocity 1 m above bottom, Lowe et al. [2005] used the velocity at 0.25 m above bottom, and Thomas and Atkinson [1997] used the surface velocity for U_{ref} in their drag parameterizations.

[28] In 3-D circulation models, the reference height for the drag parameterization varies depending on the height of the first numerical layer. As velocity varies with height above

bottom, C_D varies with reference height. To accommodate this, C_D is often specified in circulation models using a roughness length scale (e.g., z_0). This type of drag formulation typically assumes that the near-bed velocity profile is logarithmic [see *Pope*, 2000]:

$$\overline{u} = \frac{u_{*,\mathrm{eff}}}{\kappa} \ln \frac{z}{z_0}. \tag{13}$$

Reidenbach et al. [2006] found this to be a good approximation for velocity profiles in the boundary layer above coral reefs that occupy a small fraction of the water column. If the velocity profile is given by equation (13), the drag coefficient defined for reference velocity U_{ref} at height z_{ref} is related to z_0 via

$$C_D\big|^{U_{\mathrm{ref}}} = \frac{1}{U_{\mathrm{ref}}^2} \int_0^h f_{Dx}\ \gamma\ dz = \frac{u_{*,\mathrm{eff}}}{\left[{u_{*,\mathrm{eff}}}/{\kappa}\ \ln {z_{\mathrm{ref}}}/{z_0} \right]^2} = \frac{\kappa^2}{\left[\ln {z_{\mathrm{ref}}}/{z_0} \right]^2}. \tag{14}$$

Thus, C_D can be computed as a function of z_{ref}.

[29] C_D is used to parameterize spatially averaged drag (see equation (12)); thus, in equation (14), z_0 is also related to the spatially averaged drag. Typically, log profiles (equation (13)) only exist if there is a well-developed boundary layer above the roughness elements. Equation (14) therefore assumes that boundary layers are well developed and velocities are homogeneous across averaging volume, but this is often not true on reefs. In fact, velocity profiles at any given point are likely to be heavily influenced by upstream roughness elements, and spatially averaged velocity profiles are likely to have a momentum deficit in the layer containing the solid obstacles. The use of z_0 to parameterize drag on reefs where obstacles occupy a significant fraction of the water column is therefore questionable.

4. Evaluating Bulk Drag Parameterization for a Shallow Backreef

4.1. Description of Measurements

[30] The performance of the above drag parameterizations was evaluated using continuous measurements from the backreef on the north shore of Moorea, French Polynesia, made between 8 December 2006 and 16 February 2007 (Figure 1a). The average water depth is 2 m and the reef is characterized by large coral bommies (primarily *Porites* and *Pocillopora spp.*) that occupy between 0% and 90% of the water column (Figure 1b). The site does not experience significant tides due to its proximity to the M2 and K1 tidal amphidromes [*Hench et al.*, 2008]. During the austral summer, ocean swells from remote storms shoal on the steep forereef and break on the shallow (0.5 m) reef crest, generating a wave setup that forces unidirectional flow across the backreef [*Hench et al.*, 2008]. Most of the wave energy is dissipated during breaking and the small fraction of the wave energy that remains decays rapidly with distance from the reef crest. Winds are typically weak on Moorea during the Austral winter. The wind stress was estimated from measurements at Faa'a airport, on the north shore of the adjacent island of Tahiti.

[31] Pressure sensors (RBR DR-1050, sampling at 0.5 Hz) were deployed at three sites (Stations 1, 2, 3) along a cross-reef transect on the back reef to permit calculation of cross-reef surface level gradients (Figure 1a). Velocity profiles were measured at the same three sites using 2 MHz Nortek Aquadopp profilers (10 cm bins, sampling at 1 Hz, recording one profile per minute for 40 min of each hour). Time-averaged water depths at Stations 1, 2, and 3 were 1.9 m, 2.5 m, and 3.1 m, respectively. A bathymetric survey of the reef between Stations 1 and 3 indicated that the water depth varied by about ±0.5 m (1 standard deviation).

4.2. Parameterization of Drag Term in the Two-Dimensional Momentum Budget

4.2.1. Calculation of Bulk Drag Coefficient

[32] Scaling terms of the depth-averaged momentum budget (equation (3)) suggests that the momentum balance on the Moorea backreef is dominated by the cross-reef pressure gradient and drag terms (J. L. Hench, manuscript in preparation, 2011). The momentum balance can therefore be approximated as

$$-g\frac{\partial \eta}{\partial x} = \frac{C_D\big|^U U^2}{H}. \tag{15}$$

[33] Equation (4) was used to compute $C_D\big|^U$ for two backreef segments, A (Station 1 to Station 2) and B (Station 2 to Station 3). Both reef segments contain fairly dense arrays of coral bommies although the mean water depth along A is about 25% (0.6 m) shallower than for B.

[34] We evaluated equation (15) directly, from our best estimates of the spatially averaged $\partial \eta/\partial x$, U, and H for each reef segment. Reef-segment-averaged U and H values were computed as the mean of U and H at either end of the reef segment. The surface elevation gradient $\partial \eta/\partial x$ was computed from the difference between pressure sensor measurements at either end of each reef segment. Hourly averaged η, U, and H values were used for the momentum budget calculation to ensure that averages included many wave groups and averaging was performed over a timescale that was long compared with the propagation of a pressure disturbance between sites. Because the relative water depths at the three sites were unknown and flow conditions were never completely still, the absolute surface displacement at each site was estimated using an iterative method. We first assumed that the minimum water level difference between adjacent sites in the record represented no surface slope and computed an initial times series of surface slope for each reef segment. We then performed a linear regression of our initial surface slope estimate against hourly averaged U^2/H. The line of best fit was projected back to $U = 0$ to determine the "zero flow" value of $\partial \eta/\partial x$. The η values were then adjusted to reduce the "zero flow" offset in $\partial \eta/\partial x$ to zero. Our final estimate of $g\ \partial \eta/\partial x$ was then regressed against U^2/H to determine a representative $C_D\big|^U$ for each reef segment.

[35] The hourly averaged across-reef pressure gradients were strongly correlated with U^2/H for both reef segments, although the correlation was stronger further from the reef crest ($r^2 = 0.83$, and $r^2 = 0.93$ for segments A and B, respectively; Table 3 and Figure 3). RMS residuals for the

Table 3. Comparison of C_D and z_0 Values Computed From Moorea Data Using Two Different Methods: Pressure Gradient and Quadratic Drag Momentum Balances and Logarithmic Fits to Velocity Profiles[a]

U_{ref}	Segment A			Segment B		
	C_D	z_0	r^2	C_D	z_0	r^2
		Pressure Gradient and Quadratic Drag Momentum Balance				
-		0.27			0.41	
U	0.080		0.83	0.10		0.93
$\bar{u}\vert_{z=1m}$	0.073		0.83	0.10		0.93
$\bar{u}\vert_{z=0.8H}$	0.066		0.81	0.075		0.90
		Fits to Velocity Profiles				
-		9.4×10^{-4} (1)	0.996 (1)		5.9×10^{-4} (2)	0.999 (2)
		5.9×10^{-4} (2)	0.999 (2)		0.038 (3)	0.997 (3)
$\bar{u}\vert_{z=1m}$	3.5×10^{-3} (1)			3.0×10^{-3} (2)		
	3.0×10^{-3} (2)			0.016 (3)		

[a]Results are shown for three different reference velocities: depth-averaged velocity, velocity 1 m above bottom, and velocity measurement closest to water surface. Numbers in parentheses indicate measurement stations.

linear fits above were 3.8×10^{-4} m s^{-2} (22% of mean $g\,\partial\eta/\partial x$) for segment A and 1.5×10^{-4} m s^{-2} (17% of mean $g\,\partial\eta/\partial x$) for segment B. Quadratic drag coefficients from the slopes of linear fits were $C_D\vert^U = 0.08$ (A) and $C_D\vert^U = 0.10$ (B).

4.2.2. Sources of Error in C_D Estimates and Quadratic Drag Law F_D Estimates

[36] Nonlinearity in the relationship between $g\,\partial\eta/\partial x$ and U^2/H, or scatter around the linear fit, could arise from other momentum budget terms being significant or the quadratic drag law being inappropriate. For a bulk quadratic drag law to be appropriate, velocity profile shapes must be constant with time; however, for flow over an array of obstacles, velocity profile shape can be a function of flow speed [e.g., *Finnigan*, 2000]. For the Moorea backreef measurements, errors in F_D due to variations in velocity profile shape were estimated to be 5%–10%, significantly smaller than the residuals for the linear fit (Figure 3), suggesting that variations in velocity profile shapes did not explain the observed scatter in F_D estimates (see Appendix A for calculation details). For segment A, closest to the reef crest, the relationship between $g\,\partial\eta/\partial x$ and U^2/H was not quite linear, and RMS errors were somewhat larger than for segment B. This is likely because other momentum budget terms come into play at this site. The wind stress term was more than an order of magnitude smaller than other momentum budget terms; deviations from the linear fit are thought to arise mostly due to the acceleration and radiation stress terms (Hench, manuscript in preparation, 2011).

[37] The main source of uncertainty in C_D from the Moorea measurements is thought to be uncertainty in estimates of spatially averaged velocities and water depths along the reef segments. This would result in a bias in the C_D value determined, rather than causing deviation (scatter, nonlinearity) from the linear relationship between $g\,\partial\eta/\partial x$ and U^2/H. Velocities measured at a point could be consistently higher or lower than the spatial average; thus, the C_D estimates could be poor even though the quality of fits (r^2) is very high. Velocities at any point on the reef are strongly influenced by nearby obstacles; thus, point velocity measurements can be very poor estimates of spatially averaged velocities (J. L. Hench and J. H. Rosman, manuscript in preparation, 2011). The velocities used in our momentum budget calculation are averages of measurements at just two points on the reef.

Better estimates of spatially averaged velocities would be achieved by including measurements at many more points on the reef in the spatial averages; however, due to limitations in the number of sensors that can be deployed at one time, this is usually not practical (and was not in this study). We do not currently have the measurements to quantify the uncertainty in C_D due to limited spatial sampling of velocities.

4.3. Parameterization of Drag Term in the Three-Dimensional Momentum Budget

[38] Depending on the reference velocity (depth-averaged, 1 m above bottom, or near-surface) selected to parameterize drag on the Moorea backreef, $C_D\vert^{U_{\text{ref}}}$ varied from 0.066–0.080 for segment A and 0.075–0.10 for segment B (Table 3). As described above, in a 3-D model, velocity varies with z; therefore, z_0 is often specified to allow C_D to be computed from reference velocities at different heights (equation (14)). This relies on near-bottom spatially averaged velocity profiles computed by the model being logarithmic. In field and laboratory experiments, z_0 is usually determined by fitting logarithmic curves (equation (13)) to velocity profiles measured at a point in x, y [e.g., *Reidenbach et al.*, 2006].
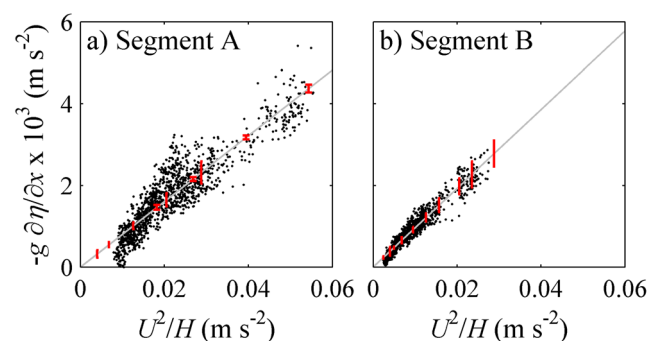

Figure 3. Scatterplots of pressure gradient force versus U^2/H for the 2 month deployment on the Moorea backreef (a) near the reef crest (segment A) and (b) far from the reef crest (segment B). Data (black dots) are 1 h averages, and gray lines are fits used to compute $C_D\vert^U$. Error bars indicate RMS error in the quadratic drag approximation due to variations in the velocity profile shape (see Appendix A).

[39] For the Moorea backreef, two deviations from the log law (equation (13)) are anticipated. First, a logarithmic velocity profile shape is only applicable to the "inner" part of the boundary layer, typically the lower 20% of the boundary layer (thickness δ), where δ is the height at which the velocity reaches the free-stream value, or the entire water column height for a fully developed velocity profile. Because the water column on the backreef is only 2–3 m and many of the measurements were above $z = 0.2\,H$, this must be taken into consideration. Above the inner layer, the outer layer velocity profile is better described by a defect law [*Coles*, 1956; *Nezu and Rodi*, 1986]. Second, for very rough boundary layers, it is not clear where $z = 0$ should be defined, thus an offset height d is typically included in the fitting function. Then d can be thought of as the height at which the net form drag affecting the velocity profile acts [*Jackson*, 1981].

[40] Combining these deviations from the log law, the velocity profile in a boundary layer (of height δ) can be described by

$$\overline{u} = \frac{u_{*,\text{eff}}}{\kappa}\left\{\ln\frac{z-d}{z_0} + 2\Pi\sin^2\left[\frac{\pi(z-d)}{2\delta}\right]\right\}. \qquad (16)$$

[41] Equation (16) has been found to fit velocity profiles in fully developed open channel flow over most of the water depth [*Nezu and Rodi*, 1986], although it does not apply very close to the surface where the zero stress boundary condition is not met. We used $\Pi = 0.2$, the value that *Nezu and Rodi* [1986] determined to be appropriate for $\text{Re}_* = u_*h/\nu > 2000$. On the Moorea backreef we estimate $\text{Re}_* \sim 10^4$ to 10^5. This Π value also gave the best quality fit (r^2) across all sites.

[42] For each Moorea backreef site, equation (16) was fit to the time-averaged velocity profile. The bottom two measurements were discarded as these values clearly deviated from fits to the measurements above them. Because δ was unknown, the curve was fit to the next three velocity measurements ($z = 0.4, 0.5, 0.6$ m). One additional velocity bin was added at a time to the fit until r^2 values began to drop as additional bins were included in the fit. The fit that included the maximum number of bins, yet maintained a high r^2, was used. Optimal fits were achieved for $z = 0.5$ m $-\,1.4$ m at Station 1, $z = 0.5$ m $-\,1.1$ m at Station 2, and $z = 0.5$ m $-\,2.2$ m at Station 3 (Table 3).

[43] C_D values computed from z_0 values (equation (14)) were an order of magnitude smaller than C_D values obtained from the cross-reef momentum balance using the same reference velocity $z_{\text{ref}} = 1$ m (Table 3). This is likely because the two C_D values represent different physical quantities. Measurement sites were selected to be away from large upstream obstacles. The z_0 values obtained from log fits to velocity profiles arise from local upstream roughness well below the height of the velocity measurements included in the fit, averaged over the length scale that the boundary layer has developed. These z_0 values do not account for form drag arising from interactions of flow with larger obstacles that are similar in size to the z range included in the log fit or drag due to variations in bottom topography at scales larger than the boundary layer development length scale. As water passes over the reef, the boundary layer is regularly disrupted by solid obstacles and must re-form. Thus, the spatially averaged velocity profile is unlikely to be logarithmic even though some portion of most velocity profiles measured at a point is logarithmic. Given that the Moorea velocity profiles are point measurements rather than spatial averages, and instrument positions were selected to avoid upstream obstacles, it is not surprising that C_D values calculated from log fit z_0 values underestimate the reef-scale drag where form drag due to large obstacles dominates overall drag.

5. Consequences of Drag Parameterization Choice

[44] The analysis of data from the Moorea backreef illustrates that C_D values derived from field data can be strongly affected by both the method used to compute them (measurement of cross-reef pressure gradient, measurement of shear stress, logarithmic fit to velocity profiles), and the reference velocity used in the drag parameterization. In addition to using different definitions, C_D values reported in the literature include the results of laboratory studies and cover a wide range of reef geometries, water depths, and flow conditions. We now develop a simple two-layer model as a conceptual framework for comparing drag coefficients in the literature and those estimated from the Moorea data.

5.1. Introduction of Two-Layer Illustrative Model

[45] We assume that the velocity profile can be approximated by two distinct layers, U_1 in an upper (obstacle-free) layer and U_2 in a lower (canopy) layer (Figure 2). We also assume that the porosity (γ), the frontal area per unit fluid volume (a) and the sectional drag coefficient (c_d) are uniform with z within the canopy layer, and that the drag term is well modeled using equation (9). Integrating equation (2) over each layer with these assumptions yields the following momentum equations:

Upper layer:

$$\frac{\partial U_1}{\partial t} + U_1\frac{\partial U_1}{\partial x} - \frac{\langle\overline{u_h}\rangle\langle\overline{w_h}\rangle}{H-h} = -g\frac{\partial\eta}{\partial x} - \frac{\tau_h}{\rho(H-h)}. \qquad (17)$$

Canopy layer:

$$\frac{\partial U_2}{\partial t} + U_2\frac{\partial U_2}{\partial x} + \frac{\langle\overline{u_h}\rangle\langle\overline{w_h}\rangle}{h} = -g\frac{\partial\eta}{\partial x} + \frac{\tau_h}{\rho h} - \frac{\frac{1}{2}c_d\lambda_F U_2^2}{\gamma h}. \qquad (18)$$

[46] The drag term has been simplified in equation (18) by carrying out the volume integral. The total frontal area of canopy elements per unit plan area is denoted $\lambda_F = \int_0^h a\,\gamma\,dz$.

[47] For steady, fully developed flow, there is a balance in the upper layer between the horizontal pressure gradient force and the stress at the top of the canopy. In the lower layer there is a balance between the pressure gradient force, the stress at the top of the canopy and the drag of the canopy elements. It can be shown, by scaling the terms in equations (17) and (18), that as h/H approaches zero, flow within the canopy is driven primarily by the shear stress at the top of the canopy. This is the situation previously considered for terrestrial canopies [*Finnigan*, 2000]. Conversely, as h/H approaches unity, within-canopy flow is driven entirely by pressure gradients [*Nepf and Vivoni*, 2000].
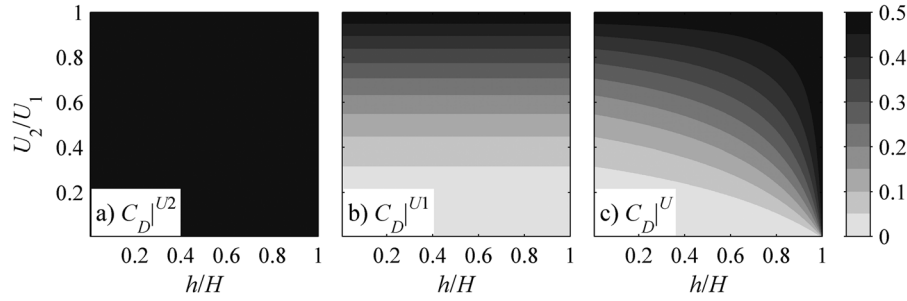
Figure 4. Contours of C_D as a function of h/H and U_2/U_1 from the two-layer model. Each plot uses a different reference velocity for the drag parameterization (a) within-canopy velocity U_2, (b) above-canopy velocity U_1, and (c) depth-averaged velocity U. All values shown correspond to $\lambda_f = 1$, $\gamma = 0.7$, and $c_d = 1$.

[48] Using the two-layer model, the expression for $C_D|^{U_{ref}}$ (equation (10)) becomes

$$C_D|^{U_{ref}} = \frac{1}{2} c_d \lambda_F \left(\frac{U_2}{U_{ref}} \right)^2. \qquad (19)$$

[49] For steady, fully developed flow, equations (17) and (18) can be combined to give an expression for the shear stress at the top of the canopy in terms of the drag within the canopy:

$$\frac{\tau_h}{\rho} = \frac{1}{2} c_d \lambda_F U_2^2 \left(1 - \frac{h}{H} \right) \equiv C_f|^{U_{ref}} U_{ref}^2. \qquad (20)$$

[50] Thus, combining equations (19) and (20) gives the following relationship between C_D and C_f,

$$\frac{C_f}{C_D} = \left(1 - \frac{h}{H} \right), \qquad (21)$$

which approaches unity for small h/H. Thus, as mentioned previously, for small h/H the values of C_D and C_f are approximately equal. From this point on, we consider only C_D.

5.2. Choice of Reference Velocity for Drag Parameterization

[51] Below, we use the two-layer model to derive an expression for C_D for three choices of U_{ref}: the upper water column velocity U_1, the within-canopy velocity U_2, and the depth-averaged velocity U.

[52] Definition I: $U_{ref} = U_2$. The simplest formulation for the bulk drag coefficient arises when U_{ref} is the within-canopy velocity. In this case, equation (19) becomes

$$C_D|^{U_2} = \frac{1}{2} c_d \lambda_F. \qquad (22)$$

[53] For this definition, the bulk drag coefficient does not depend on the canopy height, water depth, or the shape of the velocity profile (Figure 4a). If the velocity inside the canopy is known, this is the simplest model for the drag term. However, as the canopy is often too dense to permit within-canopy velocity measurements and flow fields within

canopies are spatially variable, this definition is usually not practical.

[54] Definition II: $U_{ref} = U_1$. This formulation is similar to that used in several previous studies [*Baird and Atkinson*, 1997; *Bilger and Atkinson*, 1992; *Thomas and Atkinson*, 1997]. In this case, equation (19) yields

$$C_D|^{U_1} = \frac{1}{2} c_d \lambda_F \left(\frac{U_2}{U_1} \right)^2. \qquad (23)$$

[55] Thus $C_D|^{U_1}$ depends on the canopy geometry and on the ratio of the lower and upper water column velocities (Figure 4b). While $C_D|^{U_1}$ does not depend explicitly on the ratio h/H, in practice, if the water level is varied, the shape of the velocity profile (U_2/U_1) will also vary, thus changing the value of $C_D|^{U_1}$.

[56] Definition III: $U_{ref} = U = [(H-h)U_1 + \gamma h U_2]/H_{eff}$, the depth-averaged velocity. In this case, equation (19) becomes

$$C_D|^U = \frac{1}{2} c_d \lambda_F \left(\frac{U_2}{U_1} \right)^2 \left(\frac{1 - \frac{h}{H} + \gamma \frac{h}{H}}{1 - \frac{h}{H} + \gamma \frac{h}{H} \frac{U_2}{U_1}} \right)^2. \qquad (24)$$

[57] Thus $C_D|^U$ depends on both canopy geometry (γ, h/H) and velocity profile shape (U_2/U_1) (Figure 4c). This definition of the drag coefficient reduces to the $U_{ref} = U_1$ formulation for small h/H because most of the flow is above the canopy. It reduces to the $U_{ref} = U_2$ formulation for h/H close to unity because most of the flow is through the canopy.

[58] The two-layer model illustrates that the functional form of C_D depends strongly on the choice of reference velocity. The selection of U_{ref} can result in a C_D that is independent of velocity and water column height ($U_{ref} = U_2$, Figure 4a), only dependent on the ratio of within-canopy and above canopy velocities ($U_{ref} = U_1$, Figure 4b), or strongly dependent on both the ratio of within-canopy and above canopy velocities and the ratio of canopy height to total water column height ($U_{ref} = U$, Figure 4c). In the last case, the variation in C_D spans several orders of magnitude.

5.3. Comparison of C_D Values From Different Studies

[59] Ideally, C_D values reported in the literature would be compared by converting them to a common definition. Unfortunately, in most cases, published work does not con-
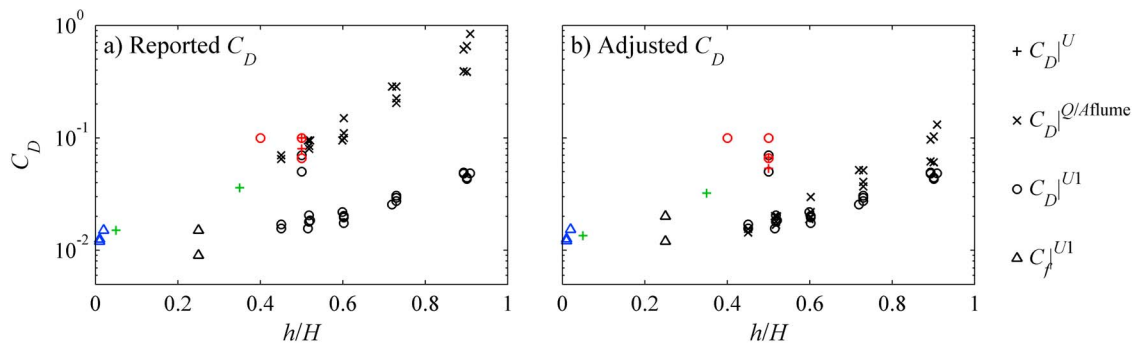
Figure 5. C_D values from the literature and from this study: (a) C_D values in Table 1 and (b) the same C_D values adjusted to a common definition ($C_D|^{U1}$) using the two-layer model with $U_2/U_1 = 0.2$ and $\gamma = 0.7$. Different symbols represent different C_D definitions. Points are color coded according to classification as laboratory flume study (black), shallow reef flat with large flow obstructions (red), shallow reef flat with smaller obstructions (green), or deeper reef where corals occupy a small fraction of the water column (blue).

tain enough information to do this comparison as it would require knowledge of spatially averaged velocity profiles from within the canopy and up into the water column, frontal area of obstacles per unit plan area as a function of z, and porosity as a function of z. In most cases, it is not practical to measure these quantities.

[60] The two-layer model provides a framework that can be used to assess the impact of C_D definition on reported C_D values. The different C_D definitions (equations (21)–(24)) differ by a factor that depends only on h/H, U_2/U_1, and γ. If these parameters were known, and the two-layer representation of $\langle \overline{u} \rangle$, a and γ was reasonable, C_D values could be converted to a common definition using the functional forms in equations (21)–(24). To illustrate the effect of C_D definition on C_D value, we used the two-layer model to convert reported C_D values to a common definition with $U_{ref} = U_1$, where U_1 is the velocity at a reference height above the layer containing solid obstacles. In cases where parameters were not known (all studies except the laboratory cylinder array study of *Lowe et al.* [2005]) we used $\gamma = 0.7$ and $U_2/U_1 = 0.2$. This conversion reduced the range of C_D values by almost an order of magnitude, from 0.009–0.8 to 0.01–0.12 (Figure 5). For field measurements over reefs with similar structures, the range in $C_D|^{U1}$ values was much smaller. $C_D|^U$ values reported by *McDonald et al.* [2006], when adjusted for definition, agreed quite well with the $C_D|^{u}_{surf}$ values we computed using their near-surface velocity measurements. It is important to note that these conversions were done for illustrative purposes only, as the true values of U_2/U_1 and γ were unknown for most studies, and the two-layer model is idealized. However, this analysis suggests that the wide range of reported C_D values is likely due, at least in part, to differences in definition.

5.4. Consequences of Using z_0 to Parameterize Drag

[61] Using the two-layer conceptual model, we now illustrate the consequences of parameterizing net drag by specifying z_0. Again, we ignore surface wind stress and horizontal shear. We assume that velocity profiles computed by a numerical model will be well described over most of the water column by a boundary layer profile consisting of an inner (log) layer and outer (log plus defect) layer. For each h/H and U_2/U_1, an effective z_0 ($z_{0,eff}$) was calculated such that

depth-integrated drag and depth-integrated mass flux were matched between a boundary layer profile shape and the two-layer flow velocity profile. This was achieved by solving for $z_{0,eff}$ in the equation,

$$\int_0^H \langle \overline{u} \rangle \, \gamma \, dz = \int_{z_{0,eff}}^H \frac{u_{*,eff}}{\kappa} \left[\ln\left(\frac{z}{z_{0,eff}}\right) + 2\Pi \sin^2\left(\frac{\pi z}{2H}\right) \right] \, dz$$

$$\approx \frac{u_{*,eff} H}{\kappa} \left[\ln\left(\frac{H}{z_{0,eff}}\right) - 1 + \Pi \right], \quad (25)$$

where, in this case, $\langle \overline{u} \rangle$ represents the two-layer model velocity and $u_{*,eff}$ is the effective shear velocity which is related to the depth-integrated drag by

$$u_{*,eff}^2 = \int_0^h f_{Dx} \, \gamma \, dz \approx \int_0^h \frac{1}{2} c_d \, a \, \langle \overline{u} \rangle^2 \, \gamma \, dz. \quad (26)$$

[62] The effective z_0 required to match both depth-integrated drag and depth-integrated mass flux for the two-layer model is shown as a function of h/H and U_2/U_1 in Figure 6. Although velocity profile shapes are not well represented by the logarithmic fits (Figure 6a), the net drag and the net mass flux are matched by using the z_0 in Figure 6b.
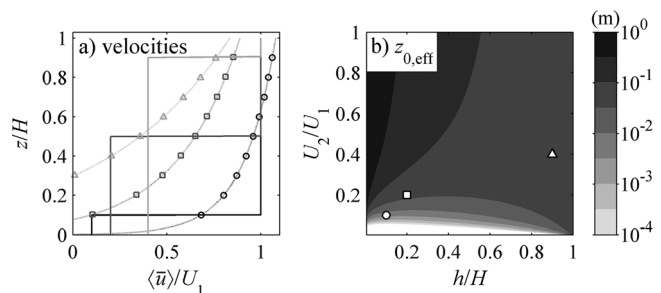

Figure 6. (a) Two-layer velocity profiles for three different h/H and U_2/U_1 ratios and the corresponding logarithmic velocity profiles that match both the depth-integrated drag and depth-integrated velocity. (b) Effective z_0 versus h/H and U_2/U_1. Symbols are values for the velocity profiles in Figure 6a.
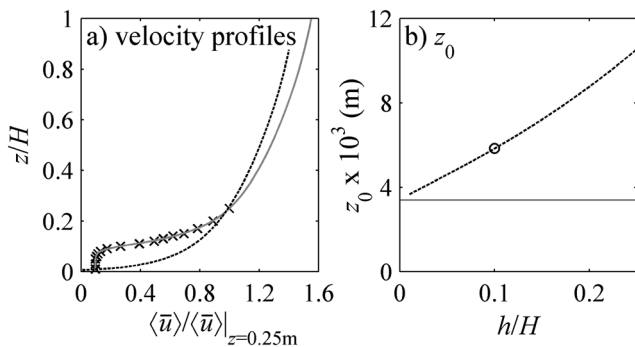
Figure 7. (a) Velocity data from *Lowe et al.* [2005] with $\lambda_f = 0.5$ and $\gamma = 0.8$ (crosses), fit to data extrapolated using a Coles defect function to $z = 1$ m (gray) and the log profile required to match depth-integrated drag and mass flux for $h/H = 0.1$ (black dashed). (b) The $z_{0,\text{eff}}$ required to match bottom drag and mass flux versus h/H (black dashed) and z_0 corresponding to the data fit to $z > h$ (gray). The circle corresponds to the case shown in Figure 7a.

Thus, z_0 values could be selected such that depth-integrated velocities and water levels were computed correctly by a circulation model; however, the vertical profiles of these velocities would be incorrect. In many cases, the z_0 values required to give sufficient drag in a circulation model may physically seem unrealistically large.

[63] The two-layer model presented above is useful for illustrative purposes; however, it was assumed that the spatially averaged velocity was uniform in the vertical, within the canopy layer (U_2) and above the canopy (U_1), and that the porosity and frontal area within the coral canopy was not a function of z. In reality, canopy density varies with z and velocity varies continuously over the water depth. The spatially averaged velocity profile is typically characterized by a shear layer at the top of the canopy which transitions to a boundary layer above the canopy [e.g., *Ghisalberti and Nepf*, 2004; *Lowe et al.*, 2005]. The top part of the canopy therefore has a greater contribution to the net drag than lower in the canopy where velocities are smaller. For example, *Reidenbach et al.* [2007] found that there was actually very little flow through most of a *P. compressa* canopy with $h/H = 0.4$.

[64] In order to illustrate the relationship between the effective z_0 (required to compute water levels correctly and conserved mass flux in a circulation model) and the z_0 that

would be determined from log fits to velocity profiles above a canopy, effective z_0 were computed from velocity profile measurements over an array of regularly spaced cylinders from *Lowe et al.* [2005] (Figure 7). Within-canopy velocity measurements were fit using a hyperbolic tangent profile, and above-canopy velocity measurements were fit with a logarithmic profile, with a transition region between the two regions where both functions decayed exponentially. The ratio h/H was artificially decreased by maintaining the bottom 25 cm of the fit and progressively increasing the extent of the boundary layer above the canopy using the form in equation (18). Equation (26) was then solved to compute $z_{0,\text{eff}}$ for each h/H. As the ratio h/H decreases (i.e., as the coral canopy occupies a smaller fraction of the water column), the computed $z_{0,\text{eff}}$ approaches the z_0 from the fit to measurements above the canopy (Figure 7b). Thus, parameterizing drag by specifying a $z_{0,\text{eff}}$ can provide reliable information about 3-D velocity fields above a coral canopy if the canopy layer occupies a small fraction of the water column and the region of interest is well above the canopy.

[65] If the coral canopy occupies a small fraction of the water column and the flow and bottom topography are homogeneous, the z_0 value obtained from log fits to measured velocity profiles above the roughness layer should match the z_0 value required to correctly implement bottom drag. However, if larger scale roughness dominates drag within a circulation model grid cell, logarithmic fits to near-bottom velocity measurements will result in z_0 values that underestimate bottom drag.

[66] The $z_{0,\text{eff}}$ that would be required to match both depth-integrated drag and mass flux were computed for the Moorea data by solving for $z_{0,\text{eff}}$ in equation (27), with $u_{*,\text{eff}}/U = (C_D|^U)^{1/2}$ determined from the across-reef momentum balance (equation (15)) as described earlier. Time-averaged velocity profiles, fits to velocity profiles, and profiles determined by matching both depth-integrated drag and depth-integrated mass flux are compared in Figure 8. For all stations, the effective velocity profile shape is quite different from the measured profile shape. This illustrates that velocity profiles computed using effective z_0 that correctly parameterize drag will not match actual velocity profiles on coral reefs, if roughness elements occupy a significant fraction of the water column. This is likely because (1) velocity fields are spatially heterogeneous and velocity profiles at a point do not represent a spatial average and (2) in shallow water, log velocity profiles measured at a point do not include form drag due to large-scale roughness. Log fits to velocity profiles will
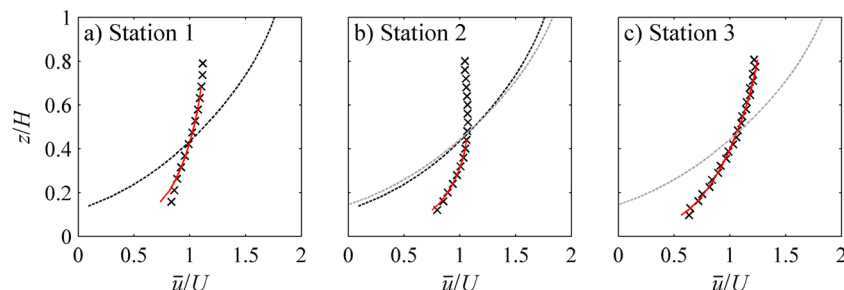

Figure 8. Comparison between measured time-averaged cross-reef velocity profiles (crosses), profiles from log fits to measurements (red), and log profiles with z_0 selected to match total drag and depth-integrated mass flux (black dashed, reef segment A; gray dashed, reef segment B).
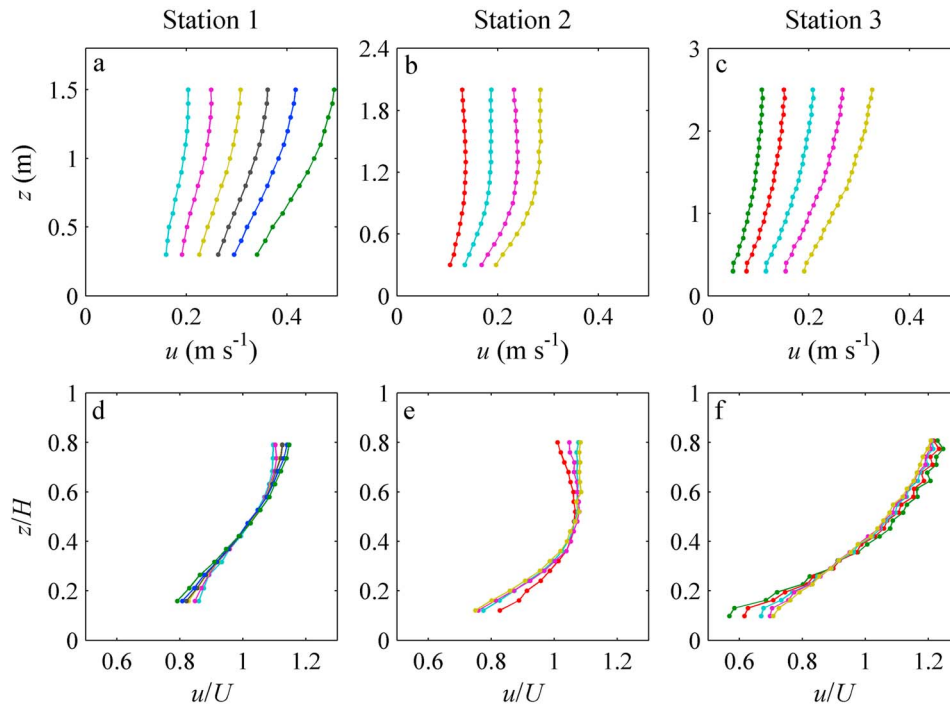
Figure A1. Measured velocity profiles on the Moorea backreef, binned and averaged according to depth-averaged velocity in 0.05 m s^{-1} intervals. (a, d) Station 1 was 50 m from reef crest, (b, e) Station 2 was 160 m from reef crest, and (c, f) Station 3 was 720 m from reef crest. Figures A1a–A1c are bin-averaged velocity profiles, and Figures A1d–A1f are bin-averaged velocities normalized by depth-averaged velocity.

only give z_0 values that provide reasonable drag in a circulation model if the length scale over which the boundary layer develops is similar to the size of a grid cell, or if velocity profiles and bottom roughness are homogeneous over the dimensions of a grid cell.

6. Conclusions

[69] At present, in most ocean circulation models, bottom drag is parameterized using bulk drag coefficients (C_D) or roughness length scales (z_0); however, reported C_D values for coral reefs span two orders of magnitude posing a challenge for predictive modeling. In this paper, we developed expressions that relate C_D and z_0 to terms in the 3-D spatially averaged momentum budget and illustrated that C_D is a function of both canopy geometry and velocity profile shape. Using an idealized two-layer model we illustrated that C_D can vary by more than an order of magnitude for the same geometry and flow, depending on the drag law reference velocity selected. While only illustrative, this analysis suggests that the range in reported C_D could be significantly reduced (by about one order of magnitude) if C_D values could be converted to a common definition.

[70] In 3-D circulation models, drag is typically parameterized by specifying z_0 as this allows C_D to be adjusted for drag law reference height. However, this type of drag parameterization relies on spatially averaged velocity profiles being logarithmic near the bed, which is often not the case on coral reefs, particularly if solid obstacles occupy a significant fraction of the water column. For the Moorea backreef, z_0 values estimated from velocity profile fits were an order of magnitude smaller than z_0 values required to correctly

parameterize net drag and maintain mass conservation. This is probably because z_0 values derived from velocity profile fits did not account for form drag arising from large obstacles in the reef segment that were further upstream than the boundary layer development length scale.

[71] A more sophisticated model that includes parameterizations for vertically distributed drag and shear stresses is required to compute 3-D velocity fields over reefs, particularly when roughness length scales are large compared with boundary layer development length scales. This is challenging as there is often a wide range of roughness length scales on reefs, from individual branches and small colonies (1–10 cm), to large colonies and aggregates (1–10 m), to reef-scale topographic variations (10–100 m). Additionally, computational grid cells can contain variations in water depth, patchiness in roughness densities, and large-scale gradients in water velocities; thus, spatial averaging procedures may need to be more complex than those discussed here. Surface waves further complicate bottom drag parameterization. Further progress on coral reef hydrodynamics will depend, in part, on a careful treatment of bottom drag and new field, laboratory and numerical studies are needed to identify the most effective drag parameterizations. In the meantime, we urge caution when using published C_D and z_0 values for coral reefs.

Appendix A: Error in Quadratic Drag Estimates Due to Variations in Velocity Profile Shapes

[72] For a bulk quadratic drag parameterization based on a reference velocity at a fixed height (or the depth-average
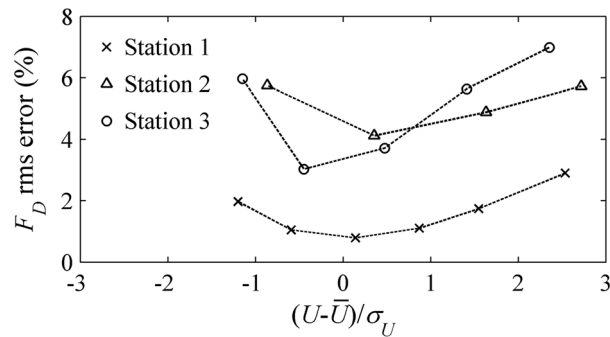
Figure A2. Errors in depth-averaged drag (F_D) due to variations in velocity profile shape if F_D is computed using a bulk drag coefficient parameterization. Errors were computed for 1 min average velocity profiles, and the RMS error for all 1 min profiles within each velocity bin in Figure 3 is shown.

velocity) to be reasonable, the velocity profile shape must not vary with flow speed, since

$$\frac{H \, F_D}{U_{\mathrm{ref}}^2} = C_D|^{U_{\mathrm{ref}}} = \int_0^h \frac{1}{2} \, c_d a \left(\frac{\langle \overline{u} \rangle}{U_{\mathrm{ref}}} \right)^2 \gamma \, dz, \qquad (A1)$$

and for a given averaging volume $c_d a$ and γ are fixed.

[73] To assess the error in quadratic drag law F_D estimates due to variations in velocity profile shapes, 1 min averaged velocity profiles were binned according to depth-averaged velocity and averaged in time to obtain mean velocity profiles for different flow speeds (Figures A1a, A1c, and A1e). Velocity profile shapes normalized by depth-averaged flow speeds were remarkably consistent, but there was an approximately 10% variation in normalized velocity profiles near-surface and near-bottom at Stations 1 and 2, and an approximately 20% variation near-bottom at Station 3 (Figures A1b, A1d, and A1f).

[74] $C_D|^U$ values (equation (A1)) computed using actual 1 min averaged velocity profile shapes were then compared with values computed using the time-averaged velocity profile shape for the whole record. For this calculation, an estimate of the $c_d a$ profile was required. As bommie heights range from 10% to 90% of the water column, and the mean bommie height is typically around half the water depth, the $c_d a$ profile was estimated as

$$c_d a = (c_d a)_0 \, e^{-z/l}, \qquad (A2)$$

where $(c_d a)_0$ represents the value of $c_d a$ at $z = 0$ and the decay length l was chosen to be 0.5 m. The RMS difference between $C_D|^U$ computed using 1 min averaged velocity profile shapes and $C_D|^U$ computed using the time-averaged velocity profile shape was then calculated for each 5 cm/s velocity bin. When converted to a percentage, this is equivalent to the percent error in the drag term (F_D) due to variations in velocity profile shapes, if a constant C_D is used. The RMS deviation of F_D estimates from values computed using the overall mean profile was greatest when velocities were either smallest or largest (i.e., when velocity profile shapes showed greatest deviation from the mean profile shape) but did not exceed 10% at either site (Figure A2).

Notation

a frontal area of solid obstacles per unit fluid volume.

A_{flume} total cross-sectional area of flume (width × water depth).

C_D bulk drag coefficient.

c_d sectional drag coefficient.

$C_D|^{U\mathrm{ref}}$ bulk drag coefficient to parameterize net drag force, reference velocity U_{ref}.

$C_f|^{U\mathrm{ref}}$ friction coefficient to parameterize shear stress at top of canopy, ref. vel. U_{ref}.

d displacement height in logarithmic velocity profile.

f_{Fx} form drag force per unit fluid mass, x direction.

f_{Vx} viscous drag force per unit fluid mass, x direction.

f_{Dx} total drag force per unit fluid mass ($f_{Fx} + f_{Vx}$), x direction.

F_D drag term in depth-averaged momentum budget.

g acceleration due to gravity (9.81 m s^{-2}).

h coral canopy height.

H water column height.

H_{eff} effective water column height, fluid volume per unit plan area.

n_x, n_y, n_z unit normal to solid surface in x, y, z directions.

n Manning's n.

p pressure.

R linear drag coefficient.

Q volumetric flow rate.

u, v, w velocity components in x, y, z directions.

$u_{*,\mathrm{eff}}$ effective shear velocity (corresponding to $\tau_{\mathrm{b,eff}}$).

U depth-averaged velocity over complete water column.

U_{ref} reference velocity (depth-integrated or at some height above bottom).

U_1 depth-averaged velocity in upper (obstacle-free) layer.

U_2 depth-averaged velocity in lower (canopy) layer.

x, y, z coordinate system directions.

z_0 roughness length scale corresponding to log fit to velocity profile.

$z_{0,\mathrm{eff}}$ roughness length scale chosen to match net bottom drag and depth-averaged mass flux.

γ porosity (fluid volume divided by total volume within averaging cuboid, Γ_{fl}/Γ).

Γ total volume of cuboid within which averaging is performed.

Γ_{fl} volume of fluid within cuboid over which averaging is performed.

δ boundary layer thickness.

η free surface elevation.

κ Von Karman constant (0.41).

λ_F frontal area of canopy elements per unit plan area.

μ molecular dynamic viscosity of seawater (1 × 10^{-3} kg m^{-1} s^{-1}).

ν molecular kinematic viscosity of seawater (1 × 10^{-6} m^2 s^{-1}).

Π Coles parameter expressing strength of log law defect function.

ρ density of water.

σ_U standard deviation of depth-averaged velocity.

$\tau_{b,\text{eff}}$ effective bottom shear stress (representing net bottom drag).

τ_h shear stress at the top of the canopy.

$^-$ (overbar) time average.

$\langle\rangle$ spatial average.

$'$ deviation from time average.

$''$ deviation from spatial average.

$\sim$ deviation from depth average.

References

Baird, M. E., and M. J. Atkinson (1997), Measurement and prediction of mass transfer to experimental coral reef communities, *Limnol. Oceanogr.*, 42(8), 1685–1693, doi:10.4319/lo.1997.42.8.1685.

Baird, M. E., M. Roughan, R. W. Brander, J. H. Middleton, and G. J. Nippard (2004), Mass-transfer-limited nitrate uptake on a coral reef flat, Warraber Island, Torres Strait, Australia, *Coral Reefs*, 23, 386–396, doi:10.1007/s00338-004-0404-z.

Bilger, R. W., and M. J. Atkinson (1992), Anomalous mass transfer of phosphate on coral reef flats, *Limnol. Oceanogr.*, 37(2), 261–272, doi:10.4319/lo.1992.37.2.0261.

Chang, S. (2007), Small-scale flow variability inside branched coral colonies: Computations and experimental validation, Ph.D. thesis, Stanford Univ., Stanford, Calif.

Cheng, H., and I. P. Castro (2002), Near wall flow over urban-like roughness, *Boundary Layer Meteorol.*, 104, 229–259, doi:10.1023/A:1016060103448.

Coceal, O., and S. E. Belcher (2004), A canopy model of mean winds through urban areas, *Q. J. R. Meteorol. Soc.*, 130, 1349–1372, doi:10.1256/qj.03.40.

Coles, D. (1956), The law of the wake in the turbulent boundary layer, *J. Fluid Mech.*, 1, 191–226, doi:10.1017/S0022112056000135.

Coronado, C., J. Candela, R. Inglesias-Prieto, J. Sheinbaum, M. López, and F. J. Ocompo-Torres (2007), On the circulation in the Puerto Morelos fringing reef lagoon, *Coral Reefs*, 26, 149–163, doi:10.1007/s00338-006-0175-9.

Cowen, R. K., and S. Sponaugle (2009), Larval dispersal and marine population connectivity, *Annu. Rev. Mater. Sci.*, 1, 443–466, doi:10.1146/annurev.marine.010908.163757.

Finnigan, J. (2000), Turbulence in plant canopies, *Annu. Rev. Fluid Mech.*, 32, 519–571, doi:10.1146/annurev.fluid.32.1.519.

Ghisalberti, M., and H. M. Nepf (2004), The limited growth of vegetated shear layers, *Water Resour. Res.*, 40, W07502, doi:10.1029/2003WR002776.

Grant, W. D., and O. S. Madsen (1979), Combined wave and current interaction with a rough bottom, *J. Geophys. Res.*, 84(C4), 1797–1808, doi:10.1029/JC084iC04p01797.

Gross, T. F., and A. R. M. Nowell (1983), Mean flow and turbulence scaling in a tidal boundary layer, *Cont. Shelf Res.*, 2(2–3), 109–126, doi:10.1016/0278-4343(83)90011-0.

Hearn, C. J. (1999), Wave-breaking hydrodynamics within coral reef systems and the effect of changing relative sea level, *J. Geophys. Res.*, 104(C12), 30,007–30,019, doi:10.1029/1999JC900262.

Hench, J. L., J. J. Leichter, and S. G. Monismith (2008), Episodic circulation and exchange in a wave-driven coral reef and lagoon system, *Limnol. Oceanogr.*, 53(6), 2681–2694, doi:10.4319/lo.2008.53.6.2681.

Jackson, P. S. (1981), On the displacement height in the logarithmic velocity profile, *J. Fluid Mech.*, 111, 15–25, doi:10.1017/S0022112081002279.

Jones, N. L., R. J. Lowe, G. Pawlak, D. A. Fong, and S. G. Monismith (2008), Plume dispersion on a fringing coral reef system, *Limnol. Oceanogr.*, 53(5, part 2), 2273–2286, doi:10.4319/lo.2008.53.5_part_2.2273.

Kaandorp, J. A., E. A. Koopman, P. M. A. Sloot, R. P. M. Bak, M. V. A. Vermeij, and L. E. H. Lampmann (2003), Simulation and analysis of flow patterns around the scleractinian coral *Madracis mirabilis* (Duchassaing and Michelotti), *Philos. Trans. R. Soc. London, Ser. B*, 358, 1551–1557, doi:10.1098/rstb.2003.1339.

Kraines, S. B., T. Yanagi, M. Isobi, and H. Komiyama (1998), Wind-wave driven circulations on the coral reef at Bora Bay, Miyako Island, *Coral Reefs*, 17, 133–143, doi:10.1007/s003380050107.

Kraines, S. B., A. Suzuki, T. Yanagi, M. Isobe, X. Guo, and H. Komiyama (1999), Rapid water exchange between the lagoon and the open ocean at Majuro Atoll due to wind, waves, and tide, *J. Geophys. Res.*, 104(C7), 15,635–15,653, doi:10.1029/1999JC900065.

Kundu, P. K. (1990), *Fluid Mechanics*, 638 pp., Academic, San Diego, Calif.

Kunkel, C. M., R. W. Hallberg, and M. Oppenheimer (2006), Coral reefs reduce tsunami impact in model simulations, *Geophys. Res. Lett.*, 33, L23612, doi:10.1029/2006GL027892.

Lowe, R. J., J. R. Koseff, and S. G. Monismith (2005), Oscillatory flow through submerged canopies: 1. Velocity structure, *J. Geophys. Res.*, 110, C10016, doi:10.1029/2004JC002788.

Lowe, R. J., J. L. Falter, S. G. Monismith, and M. J. Atkinson (2009), Wave-driven circulation of a coastal reef–lagoon system, *J. Phys. Oceanogr.*, 39(4), 873–893, doi:10.1175/2008JPO3958.1.

Lugo-Fernández, A., H. H. Roberts, W. J. Wiseman Jr., and B. L. Carter (1998), Water level and currents of tidal and infragravity periods at Tague Reef, St. Croix (USVI), *Coral Reefs*, 17, 343–349, doi:10.1007/s003380050137.

McDonald, C. B., J. R. Koseff, and S. G. Monismith (2006), Effects of the depth to coral height ratio on drag coefficients for unidirectional flow over coral, *Limnol. Oceanogr.*, 51(3), 1294–1301, doi:10.4319/lo.2006.51.3.1294.

Monismith, S. G. (2007), Hydrodynamics of coral reefs, *Annu. Rev. Fluid Mech.*, 39, 37–55, doi:10.1146/annurev.fluid.38.050304.092125.

Nepf, H. M. (1999), Drag, turbulence, and diffusion in flow through emergent vegetation, *Water Resour. Res.*, 35(2), 479–489, doi:10.1029/1998WR900069.

Nepf, H. M., and E. R. Vivoni (2000), Flow structure in depth-limited, vegetated flow, *J. Geophys. Res.*, 105(C12), 28,547–28,557, doi:10.1029/2000JC900145.

Nezu, I., and W. Rodi (1986), Open-channel flow measurements with a laser Doppler anemometer, *J. Hydraul. Eng.*, 112, 335–355, doi:10.1061/(ASCE)0733-9429(1986)112:5(335).

Nikora, V., I. McEwan, S. McLean, S. Coleman, D. Pokrajac, and R. Walters (2007), Double-averaging concept for rough bed open channel and overland flows: Theoretical background, *J. Hydraul. Eng.*, 133(8), 873–883, doi:10.1061/(ASCE)0733-9429(2007)133:8(873).

Nunes, V., and G. Pawlak (2008), Observations of bed roughness of a coral reef, *J. Coastal Res.*, 24, 39–50, doi:10.2112/05-0616.1.

Pope, S. B. (2000), *Turbulent Flows*, 771 pp., Cambridge Univ. Press, Cambridge, U. K.

Prager, E. J. (1991), Numerical simulation of circulation in a Caribbean-type backreef lagoon, *Coral Reefs*, 10, 177–182, doi:10.1007/BF00336771.

Raupach, M. R., and A. S. Thom (1981), Turbulence in and above plant canopies, *Annu. Rev. Fluid Mech.*, 13, 97–129, doi:10.1146/annurev.fl.13.010181.000525.

Reidenbach, M. A., S. G. Monismith, J. R. Koseff, G. Yahel, and A. Genin (2006), Boundary layer turbulence and flow structure over a fringing coral reef, *Limnol. Oceanogr.*, 51(5), 1956–1968, doi:10.4319/lo.2006.51.5.1956.

Reidenbach, M. A., J. R. Koseff, and S. G. Monismith (2007), Laboratory experiments of fine-scale mixing and mass transport within a coral canopy, *Phys. Fluids*, 19, doi:10.1063/1.2752189.

Roberts, H. H., S. P. Murray, and J. H. Suhayda (1975), Physical processes in a fringing reef system, *J. Mar. Res.*, 33, 233–260.

Sebens, K. P., S. P. Grace, B. Helmuth, E. J. Maney Jr., and J. S. Miles (1998), Water flow and prey capture by three scleractinian corals, *Madracis mirabilis, Montastrea cavernosa,* and *Porites porites* in a field enclosure, *Mar. Biol. Berlin*, 131, 347–360, doi:10.1007/s002270050328.

Sternberg, R. W. (1968), Friction factors in tidal channels with differing bed roughness, *Mar. Geol.*, 6, 243–260, doi:10.1016/0025-3227(68)90033-9.

Symonds, G., K. P. Black, and I. R. Young (1995), Wave-driven flow over shallow reefs, *J. Geophys. Res.*, 100(C2), 2639–2648, doi:10.1029/94JC02736.

Tamura, H., K. Nadaoka, and E. C. Paringit (2007), Hydrodynamic characteristics of a fringing coral reef on the east coast of Ishigaki Island, southwest Japan, *Coral Reefs*, 26, 17–34, doi:10.1007/s00338-006-0164-z.

Tartinville, B., E. Deleersnijder, and J. Rancher (1997), The water residence time in the Mururoa atoll lagoon: Sensitivity analysis of a three-dimensional model, *Coral Reefs*, 16, 193–203, doi:10.1007/s003380050074.

Tarya, A., A. J. F. Hoitink, and M. Van der Vegt (2010), Tidal and subtidal flow patterns on a tropical continental shelf semi-insulated by coral reefs, *J. Geophys. Res.*, 115, C09029, doi:10.1029/2010JC006168.

Thomas, F. I. M., and M. J. Atkinson (1997), Ammonium uptake by coral reefs: Effects of water velocity and surface roughness on mass transfer, *Limnol. Oceanogr.*, *42*(1), 81–88, doi:10.4319/lo.1997.42.1.0081.

Todd, P. A. (2008), Morphological plasticity in scleractinian corals, *Biol. Rev.*, *83*(3), 315–337, doi:10.1111/j.1469-185X.2008.00045.x.

Young, I. R., K. P. Black, and M. L. Heron (1994), Circulation in the Ribbon Reef region of the Great Barrier Reef, *Cont. Shelf Res.*, *14*(2–3), 117–142, doi:10.1016/0278-4343(94)90009-4.

Zawada, D. G., G. A. Piniak, and C. J. Hearn (2010), Topographic complexity and roughness of a tropical benthic seascape, *Geophys. Res. Lett.*, *37*, L14604, doi:10.1029/2010GL043789.

J. L. Hench, Duke University Marine Laboratory, Nicholas School of the Environment, 135 Marine Lab Rd., Beaufort, NC 28516, USA.

J. H. Rosman, Institute of Marine Sciences, University of North Carolina at Chapel Hill, 3431 Arendell St., Morehead City, NC 28557, USA. (jrosman@email.unc.edu)